A method for analyzing how various parts of clouds influence each other's brightness

Tamás Várnai and Alexander Marshak[1]

Joint Center for Earth Systems Technology, University of Maryland Baltimore County, Baltimore, Maryland, USA

Received 4 March 2003; revised 3 July 2003; accepted 28 July 2003; published 29 November 2003.

[1] This paper proposes a method for obtaining new information on three-dimensional (3-D) radiative effects that arise from horizontal radiative interactions in heterogeneous clouds. Unlike current radiative transfer models, it can not only calculate how 3-D effects change radiative quantities at any given point but can also determine which areas contribute to these 3-D effects, to what degree, and through what mechanisms. The new method uses Monte Carlo radiative transfer simulations to generate numerous photon trajectories through the cloud field, and then it examines the radiative processes along each trajectory. After describing the proposed method, the paper illustrates its new capabilities both for detailed case studies and for the statistical processing of large data sets. Because the proposed method makes it possible, for the first time, to link a particular change in cloud properties to the resulting 3-D effect, it can be used to develop new types of radiative transfer parameterizations. Encouraging initial results suggest that such parameterizations will be able to incorporate 3-D effects in practical applications currently limited to 1-D theory, such as remote sensing of cloud properties and dynamical cloud modeling. *INDEX TERMS:* 3359 Meteorology and Atmospheric Dynamics: Radiative processes; 0320 Atmospheric Composition and Structure: Cloud physics and chemistry; *KEYWORDS:* clouds, solar radiation, three-dimensional

Citation: Várnai, T., and A. Marshak, A method for analyzing how various parts of clouds influence each other's brightness, *J. Geophys. Res.*, *108*(D22), 4706, doi:10.1029/2003JD003561, 2003.

1. Introduction

[2] Current practical applications of calculating solar radiative transfer in clouds, such as cloud remote sensing and dynamical cloud models, rely on one-dimensional (1-D) radiative transfer theory. This means that the calculations do not consider horizontal processes, that is, the 3-D radiative interactions among areas that have different cloud properties. Unfortunately, although the 1-D assumption makes the calculations much more simple and fast, it can also cause significant errors in the case of heterogeneous clouds. For example, 1-D cloud property retrievals based on satellite measurements can yield clouds that are too thin or too thick, too smooth or too structured, artificially anisotropic, or asymmetric [e.g., *Marshak et al.*, 1995; *Loeb and Davies*, 1996; *Zuidema and Evans*, 1998; *Várnai and Marshak*, 2002]. In addition, 1-D calculations can have large errors in calculations of radiative fluxes and absorption values [e.g., *Davies et al.*, 1984; *Barker and Davies*, 1992; *Marshak et al.*, 1999; *Benner and Evans*, 2001], thus resulting in inaccurate radiative heating rates in dynamical cloud models [e.g., *O'Hirok and Gauthier*, 1998; *Barker et al.*, 1998]. Finally, 3-D effects can also influence some chemical processes by changing the actinic fluxes that affect photodissociation rates [*Los et al.*, 1997].

[3] Ever since the first theoretical studies raised the issue of 3-D radiative effects in the mid-1970s [*Busygin et al.*, 1973; *McKee and Cox*, 1974], theoretical calculations have provided numerous important insights into these effects. The theoretical studies calculated the 3-D effects indirectly, by comparing results when 3-D effects were taken into account and when they were not. Unfortunately, this indirect approach of detecting 3-D effects from their imprint on the calculated radiation fields puts some limitations on the information that can be obtained. For example, although the calculations can determine the overall influence of 3-D effects on the brightness of a particular pixel, they cannot quantitatively address questions about their causes: Why is a certain pixel as bright as it is? What other pixels influence its brightness, to what degree, and through what mechanisms?

[4] Despite these limitations, studies using the indirect approach yielded a wealth of information on the causes and mechanisms of 3-D radiative effects. For example, the analysis of flux lines in simple cloud structures (such as a sine wave or a single perturbation in a homogeneous environment) revealed the way thick areas channel radiation toward thinner regions [e.g., *Davis and Marshak*, 2001]. In addition, the Fourier analysis of complex cloud fields revealed the scales at which 3-D effects change the structure of radiance fields, for example, by smoothing out small-scale variability through radiative diffusion [e.g., *Marshak*

[1]Now at Climate and Radiation Branch, NASA Goddard Space Flight Center, Greenbelt, Maryland, USA.

0148-0227/03/2003JD003561$09.00

et al., 1995; *Davis et al.*, 1997; *Oreopoulos et al.*, 2000]. Such results, however, can be related to physical processes only with some caution, because 3-D radiative interactions that occur at one particular scale and direction can change the variability of radiance fields at other scales and directions [e.g., K. Frank Evans, personal communication, 1998; *Várnai*, 2000]. Recently, *Fauré et al.* [2001a] used neural network analysis to estimate the overall influence of 3-D effects on a pixel by assigning "weights of importance" to all surrounding pixels. Although this novel approach may lead to some capable new remote sensing methods [*Fauré et al.*, 2001b], the paper cautioned readers about interpreting these weights in terms of physical processes: The weight values depend not only on the radiative interactions that occur in the cloud field but also on some arbitrary choices in the adapted neural network methodology.

[5] In contrast to current, indirect methods, this paper presents a theoretical approach that can detect 3-D effects directly as they modify the flow of radiation inside the cloud field. As a result, the proposed technique can not only calculate the combined effect a pixel's surroundings have on its brightness but can also determine how specific pixels contribute to the combined effect, to what degree, and through what mechanisms.

[6] In examining the flow of radiation inside cloud fields, the proposed technique is related to the approach developed by *Várnai and Davies* [1999]. However, while that approach examined radiative processes only in a scene-averaged sense, the technique proposed here can also give information on the spatial distribution of 3-D radiative effects.

[7] In addition to providing us a more thorough understanding of 3-D radiative processes, in future studies the proposed method can also help us interpret remote sensing measurements and develop parameterizations of 3-D radiative fluxes and absorption values for dynamical cloud models.

[8] The outline of this paper is as follows: First, section 2 describes the proposed theoretical approach, then section 3 illustrates the method's capabilities and potential uses through several examples. Finally, section 4 offers a brief summary and some concluding remarks.

2. Proposed Technique

2.1. Basic Definitions

[9] Although the proposed approach can be applied to examine any radiative quantity (i.e., radiances, fluxes, and absorption values), for simplicity, this paper will describe the new technique using nadir reflectance (R) as an example. The reflectance of a pixel A is defined by the equation

$$R^A = \frac{\pi I^A}{\mu_0 F}, \tag{1}$$

where I^A is the nadir radiance at pixel A, μ_0 is the cosine of the solar zenith angle, and F is the solar irradiance. For the sake of simplicity, this reflectance will sometimes be referred to as "brightness."

[10] The influence of 3-D effects on the brightness of pixel A (ΔR^A) is then defined as

$$\Delta R^A = R^A_{3-\mathrm{D}} - R^A_{1-\mathrm{D}}, \tag{2}$$

where $R^A_{3\text{-D}}$ and $R^A_{1\text{-D}}$ are the brightnesses of A calculated using 3-D and 1-D theory, respectively. As illustrated in Figure 1, the 1-D calculations assume that the entire scene has exactly the same geometrical and optical properties as the pixel whose brightness we are to explain.

[11] In order to better explain the calculated 3-D effects, this paper identifies the mechanisms of 3-D effects by considering two questions: whether the 3-D effects enhance or reduce the flow of radiation to pixel A (relative to the 1-D case), and whether they act by causing more extinction or less. In the case of conservative scattering (i.e., no absorption or emission), the four possible combinations of answers yield the following basic mechanisms:

[12] 1. Enhancement by more scattering (EMS). In this case the extra scattering acts to channel radiation to pixel A (Figure 2a), which is part of the channeling effect described in earlier studies [e.g., *Cannon*, 1970; *Davis and Marshak*, 2001].

[13] 2. Enhancement by less scattering (ELS). In this case the reduced scattering allows more radiation to reach our pixel (Figure 2b), which is the process responsible for the side illumination effect described in earlier studies [e.g., *Wendling*, 1977; *Cahalan et al.*, 1994].

[14] 3. Reduction by more scattering (RMS). In this case the extra scattering allows less radiation to reach pixel A (Figure 2c), which is the shadowing effect described in earlier studies [e.g., *Chambers et al.*, 1997a; *Zuidema and Evans*, 1998].

[15] 4. Reduction by less scattering (RLS). In this case the reduced scattering allows some radiation to leak out of the paths leading to pixel A (Figure 2d), which is the process responsible for the leakage effect described in earlier studies [e.g., *Davies*, 1978; *Kobayashi*, 1993].

[16] Because the overall 3-D effect arises from the four mechanisms described above, one can write that

$$\Delta R^A = \Delta R^A_{\mathrm{ELS}} + \Delta R^A_{\mathrm{EMS}} + \Delta R^A_{\mathrm{RLS}} + \Delta R^A_{\mathrm{RMS}}, \tag{3}$$

where each component is the brightness change due to a single mechanism. (Note that the first two components are never negative, that is, $\Delta R^A_{\mathrm{ELS}} \geq 0$, and $\Delta R^A_{\mathrm{EMS}} \geq 0$ whereas the other two components are never positive, that is, $\Delta R^A_{\mathrm{RLS}} \leq 0$, and $\Delta R^A_{\mathrm{RMS}} \leq 0$.) Section 2.3 describes how one can calculate the magnitude of each component.

[17] Let us note that these mechanisms are substantially different from the mechanisms *Várnai and Davies* [1999] used for studying scene-averaged 3-D radiative effects. For example, *Várnai and Davies* [1999] defined the mechanisms using a separate 1-D scene for each photon (the 1-D scene had the same properties as the point where the photon entered the cloud field), whereas the new framework uses a single 1-D scene for all photon paths leading to our pixel (see Figure 1). This difference makes the new approach more suitable for practical applications in which the spatial distribution of radiation is considered (such as remote sensing or dynamical cloud modeling).

[18] The four basic mechanisms influence the brightness of individual pixels, and so they can be combined into two processes that change the structure of the brightness field by roughening or smoothing it. These two processes were described qualitatively in numerous earlier studies [e.g., *Marshak et al.*, 1995; *Davis et al.*, 1997; *Oreopoulos et al.*,

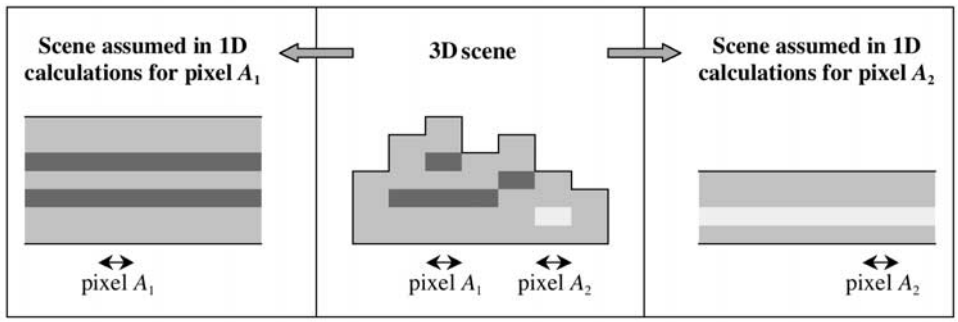

Figure 1. Illustration of the horizontally homogeneous scenes that are assumed in the 1-D calculations for each pixel. Darker shading indicates higher volume scattering coefficient. See color version of this figure in the HTML.

2000]. In order to provide quantitative definitions for these mechanisms, we need to use the scene-averaged influence of each mechanism, which will be identified by overbars.

[19] 1. Roughening. The mechanisms ELS and RMS increase the brightness difference between the influencing and influenced pixels that we would expect from 1-D theory, thereby roughening the brightness field. Because the reductions by RMS strengthen the roughening caused by ELS even though their values have opposite signs, we need to use the absolute value of RMS in defining the magnitude of roughening:

$$\text{roughening} = \overline{\Delta R_{\text{ELS}}} + \left|\overline{\Delta R_{\text{RMS}}}\right|. \tag{4a}$$

[20] 2. Smoothing. The mechanisms EMS and RLS reduce the brightness difference between the influencing and influenced pixels that we would expect from 1-D theory, thereby smoothing out the brightness field. Therefore in analogy with roughening, the magnitude of smoothing can be calculated as

$$\text{smoothing} = \overline{\Delta R_{\text{EMS}}} + \left|\overline{\Delta R_{\text{RLS}}}\right|. \tag{4b}$$

[21] These two mechanisms can in turn be combined to calculate the ''net roughening'' as

$$\text{net roughening} = \text{roughening} - \text{smoothing}. \tag{5}$$

[22] Finally, let us mention that when absorption or emission is also present, four additional basic mechanisms can also be considered: ELA, RMA, EME, and RLE, where A designates absorption and E designates emission. If present, ELA and RMA contribute to roughening, whereas EME and RLE contribute to smoothing.

2.2. Main Tasks of the Proposed Technique

[23] Unfortunately, the two seemingly most straightforward approaches, using the sensitivity of R^A to changes in the properties of pixel B and comparing the amount of extinction at B in 3-D and 1-D calculations, cannot be used to determine the 3-D influence of pixel B, because they would often yield inappropriate, ''unphysical'' results. The fundamental problem with these approaches is that they assume that each pixel acts in isolation, whereas in reality, the influence of a pixel also depends on the other pixels along the path of radiation. For example, the properties of B may have a large influence on the brightness of A if the pixels between A and B are transparent; but they may have a negligible impact if the pixels between A and B are so dense that they hardly allow any radiation through. As a result, the influence of B on A should be determined by considering

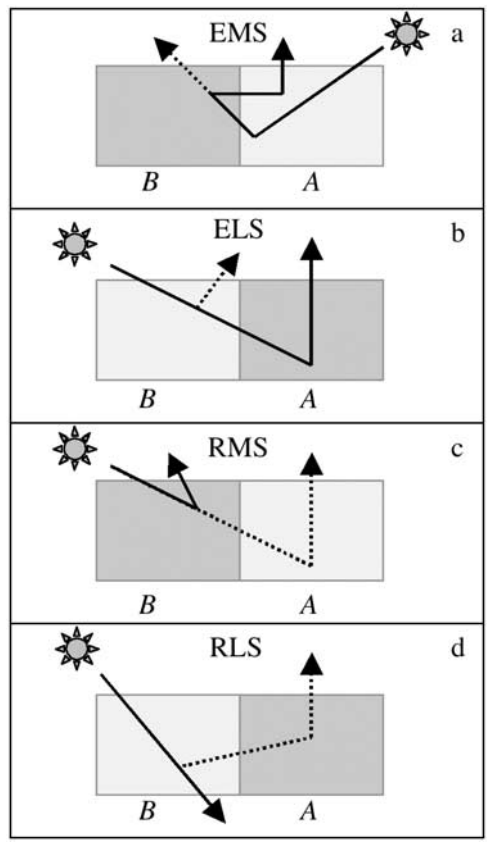

Figure 2. Examples of four mechanisms of 3-D effects influencing R^A. The solid arrows indicate the path of radiation in the 3-D cloud field; the dotted arrows indicate the path the radiation would follow in the 1-D case (in which case the entire scene, including pixel B, has the same properties as pixel A). Darker shading indicates higher volume extinction coefficient. See color version of this figure in the HTML.

not only the properties of A and B but also the entire path along which the radiation arrives from the Sun, moves to B, and then goes to A.

[24] To obtain the paths radiation follows, we need to use Monte Carlo experiments that simulate the photons' journey inside the cloud field. Therefore the proposed method needs to carry out two main tasks: First, it needs to define the paths along which radiation coming from the Sun can reach pixel A and calculate the overall influence of 3-D effects along each path. Second, it needs to determine how pixels along each path contribute to the overall 3-D effect along that path. In the end, the pixels' overall effects are obtained by combining the results calculated for each individual path. This section discusses these two tasks in detail. For simplicity, they are described for the case of conservative scattering.

2.2.1. Task 1: Define a Set of Paths Along Which Radiation Coming From the Sun Can Reach Pixel A and Calculate the Overall Influence of 3-D Effects Along Each Path

[25] The proposed method recognizes that all photon paths leading to pixel A fall into one of the two categories. The first category includes all paths along which 3-D effects enhance the flow of radiation, thereby increasing R^A, plus the paths along which 3-D effects do not change the flow. The second category includes all paths along which 3-D effects reduce the flow of radiation, thereby reducing R^A.

[26] While a 3-D Monte Carlo simulation can generate the paths for the first category, it cannot generate some of the paths in the second category. For example, 3-D simulations could not generate paths like the one in Figure 3: There are no droplets at point B in the 3-D scene, so the simulations could never put a scattering event at point B. Missing such paths would distort our results, because if we did not notice that the hole at B reduces the radiation that could flow along this path, we would not notice that B causes a 3-D effect that reduces R^A.

[27] Because the 3-D simulation could not give a suitable set of paths with reductions, a 1-D Monte Carlo simulation generates the paths for this second category instead. (Note that due to problems similar to those in Figure 3, the 1-D simulation could not generate the paths for the first category (paths with 3-D enhancements).)

[28] In order to determine which 3-D paths do belong to the first category (enhancements) and which 1-D paths do belong to the second category (reductions), we need to calculate the overall influence of 3-D effects along each simulated path. In these calculations we denote the radiation that follows a single specific path by $'$ (prime). Using this notation, equation (2) can be rewritten for individual paths as

$$\Delta R' = R'_{3-D} - R'_{1-D}. \tag{6}$$

[29] For paths generated in the 3-D simulation, $R'_{3\text{-D}}$ can be calculated using standard Monte Carlo procedures such as the method of local estimates [e.g., *Marchuk et al.*, 1980] or the use of fluxes reflected into small solid angle bins [e.g., *Wendling*, 1977; *Di Girolamo et al.*, 1998].

[30] In order to calculate the 3-D effects that occur along each path, we need to use the probability density function $k_{3\text{-D}}(\mathbf{r}_i, \mathbf{r}_{i+1}, \mathbf{\Omega}_i, \mathbf{\Omega}_{i+1})$, which describes the transition of radiative energy from point $\mathbf{r}_i$ and direction $\mathbf{\Omega}_i$ into point $\mathbf{r}_{i+1}$ and direction $\mathbf{\Omega}_{i+1}$. It follows from the integral form of the radiative transfer equation [*Marchuk et al.*, 1980, pp. 11–12] that

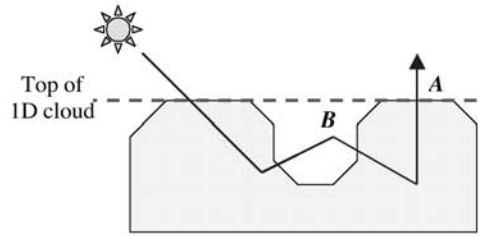

Figure 3. A path along which radiation can travel in a 1-D scene but not in a 3-D scene. See color version of this figure in the HTML.

$$k_{3\text{-D}}(\mathbf{r}_i, \mathbf{r}_{i+1}, \mathbf{\Omega}_i, \mathbf{\Omega}_{i+1}) = \exp\left[-\int_0^{|\mathbf{r}_{i+1}-\mathbf{r}_i|} \beta_{3\text{-D}}(\mathbf{r}_i + s\mathbf{\Omega}_i)ds\right] \cdot \beta_{3\text{-D}}(\mathbf{r}_{i+1}) P_{3\text{-D}}(\mathbf{r}_{i+1}, \mathbf{\Omega}_i \bullet \mathbf{\Omega}_{i+1}) \cdot \frac{1}{2\pi|\mathbf{r}_{i+1}-\mathbf{r}_i|^2} \delta\left(\mathbf{\Omega}_i - \frac{\mathbf{r}_{i+1}-\mathbf{r}_i}{|\mathbf{r}_{i+1}-\mathbf{r}_i|}\right), \tag{7}$$

where β is the volume-scattering coefficient, and P is the scattering phase function. The sign $|\ |$ indicates the length of a vector, $\bullet$ denotes the scalar product of two vectors, and δ is a Dirac-delta function. (Note that for any $\mathbf{r}_i$ and $\mathbf{\Omega}_i$, the integral of $k_{3\text{-D}}$ over the entire range of $\mathbf{r}_{i+1}$ and $\mathbf{\Omega}_{i+1}$ gives 1.) In our method we set $\mathbf{r}_i$ to be the location of the ith scattering point.

[31] After calculating the $k_{3\text{-D}}$ values for each segment of the path, we can combine them for the entire path to get $k'_{3\text{-D}}$:

$$k'_{3\text{-D}} = \prod_{i=0}^{N_s} k_{3\text{-D}}(\mathbf{r}_i, \mathbf{r}_{i+1}, \mathbf{\Omega}_i, \mathbf{\Omega}_{i+1}), \tag{8}$$

where N_s is the (random) number of scattering events along the path. In this equation, $\mathbf{r}_0$ is located at the top of the atmosphere, where the incoming sunlight enters in direction $\mathbf{\Omega}_0$. In turn, $\mathbf{r}_{N_s+1}$ is the location where the path ends (e.g., at the imaginary sensor whose observations the Monte Carlo experiment simulates), and $\mathbf{\Omega}_{N_s+1}$ is the direction the photons would keep following if the imaginary sensor had not caught them, which means that $\mathbf{\Omega}_{N_s+1} = \mathbf{\Omega}_{N_s}$. (The equations presented later in this section imply that, because of a cancellation of terms, the proposed method's final results do not depend on $\mathbf{\Omega}_{N_s+1}$.)

[32] Next, let us consider how much radiation could follow the very same geometrical path in the 1-D scene. For this, we can calculate $k'_{1\text{-D}}$ using the very same $\mathbf{r}_i$ values in the equation

$$\begin{aligned} k'_{1\text{-D}} &= \prod_{i=0}^{N_s} k_{1\text{-D}}(\mathbf{r}_i, \mathbf{r}_{i+1}, \mathbf{\Omega}_i, \mathbf{\Omega}_{i+1}) \\ &= \prod_{i=0}^{N_s} \left\{ \exp\left[-\int_0^{|\mathbf{r}_{i+1}-\mathbf{r}_i|} \beta_{1\text{-D}}(\mathbf{r}_i + s\mathbf{\Omega}_i)ds\right] \cdot \beta_{1\text{-D}}(\mathbf{r}_{i+1}) P_{1\text{-D}}(\mathbf{r}_{i+1}, \mathbf{\Omega}_i \bullet \mathbf{\Omega}_{i+1}) \frac{1}{2\pi|\mathbf{r}_{i+1}-\mathbf{r}_i|^2} \cdot \delta\left(\mathbf{\Omega}_i - \frac{\mathbf{r}_{i+1}-\mathbf{r}_i}{|\mathbf{r}_{i+1}-\mathbf{r}_i|}\right) \right\}, \end{aligned} \tag{9}$$

where $\beta_{1\text{-D}}$ and $P_{1\text{-D}}$ are the values that would occur if the entire scene had the same properties as pixel A (Figure 1), and $k_{1\text{-D}}$ is the 1-D counterpart to $k_{3\text{-D}}$ in equation (7). Then the ratio $\rho = k'_{3\text{-D}}/k'_{1\text{-D}}$ is the factor by which 3-D effects enhance (if $\rho > 1$) or reduce (if $\rho < 1$) the flow of radiation along the path. Because $R'_{3\text{-D}}$ and $R'_{1\text{-D}}$ are the amounts of radiation that actually follow the path, we can write that

$$\rho = \frac{R'_{3\text{-D}}}{R'_{1\text{-D}}} = \frac{k'_{3\text{-D}}}{k'_{1\text{-D}}} = \prod_{i=0}^{N_s} \frac{\exp\left[-\int_0^{|\mathbf{r}_{i+1}-\mathbf{r}_i|} \beta_{3\text{-D}}(\mathbf{r}_i + s\Omega_i)ds\right]\beta_{3\text{-D}}(\mathbf{r}_{i+1})P_{3\text{-D}}(\mathbf{r}_{i+1}, \Omega_i \bullet \Omega_{i+1})}{\exp\left[-\int_0^{|\mathbf{r}_{i+1}-\mathbf{r}_i|} \beta_{1\text{-D}}(\mathbf{r}_i + s\Omega_i)ds\right]\beta_{1\text{-D}}(\mathbf{r}_{i+1})P_{1\text{-D}}(\mathbf{r}_{i+1}, \Omega_i \bullet \Omega_{i+1})}. \tag{10}$$

Since we know $k'_{3\text{-D}}$, $k'_{1\text{-D}}$, and $R'_{3\text{-D}}$, we can use the equation to get both ρ and $R'_{1\text{-D}}$.

[33] Once the calculations for all the 3-D paths are done, the same procedure is used for the paths defined in the 1-D simulation, with the only difference that equation (10) is now used to get $R'_{3\text{-D}}$.

2.2.2. Task 2: Determine How Pixels Along Each Path Contribute to the Overall 3-D Effect Along That Path

[34] For each path, the influence of a pixel B can be best characterized through the value of $\rho(B)$, which considers only the 3-D effects occurring inside B. In order to ensure that $\rho(B)$ reflects only on the processes inside B, we need to "neutralize" all terms in equation (10) that refer to locations outside B by giving them a value of 1. Then

$$\rho(B) = \prod_{i=0}^{N_s} \frac{\exp\left(-\int_0^{|\mathbf{r}_{i+1}-\mathbf{r}_i|} H_B(\mathbf{r}_i + s\Omega_i)\beta_{3\text{-D}}(\mathbf{r}_i + s\Omega_i)ds\right)}{\exp\left(-\int_0^{|\mathbf{r}_{i+1}-\mathbf{r}_i|} H_B(\mathbf{r}_i + s\Omega_i)\beta_{1\text{-D}}(\mathbf{r}_i + s\Omega_i)ds\right)} \cdot \begin{cases} \dfrac{\beta_{3\text{-D}}(\mathbf{r}_{i+1})P_{3\text{-D}}(\mathbf{r}_{i+1}, \Omega_i \bullet \Omega_{i+1})}{\beta_{1\text{-D}}(\mathbf{r}_{i+1})P_{1\text{-D}}(\mathbf{r}_{i+1}, \Omega_i \bullet \Omega_{i+1})}, & \text{if } \mathbf{r}_{i+1} \in B \\ 1, & \text{if } \mathbf{r}_{i+1} \notin B. \end{cases} \tag{11}$$

where the indicator function $H_B(\mathbf{r})$ is equal to 1 if $\mathbf{r}$ is inside B, and to 0 otherwise.

[35] Unfortunately, ρ itself is not a suitable measure of a pixel's influence. The problem is that if ρ was used as is, one would not know how to combine the influences calculated for two arbitrary pixels B and C after the results for all paths had been summed up. For example, the influences of B and C should be multiplied if they affected radiation that go through both of them, whereas the influences should be added if B and C affected radiation approaching A through different paths (e.g., if B affected radiation coming from the left and C affected radiation coming from the right).

[36] To avoid this problem, we need to characterize the influence of a pixel as a function F of ρ

$$\Delta R'(B) = F[\rho(B)], \tag{12}$$

in a such way that allows additions for any pixels B and C:

$$\Delta R'(B \cup C) = \Delta R'(B) + \Delta R'(C). \tag{13}$$

Equation (11) reveals that the enhancements and reductions along a path are a multiplicative process, i.e., $\rho(B \cup C) = \rho(B)\rho(C)$, and so equation (13) implies that F needs to satisfy the equation

$$F[\rho(B \cup C)] = F[\rho(B)\rho(C)] = F[\rho(B)] + F[\rho(C)]. \tag{14}$$

By definition, it is the logarithm function that satisfies the second equality in this equation, and so F must be in the form

$$F[\rho(B)] = \kappa \log \rho(B). \tag{15}$$

The coefficient κ is needed to ensure that the sum of contributions from all pixels gives the overall 3-D effect along the path. That is, if pixels B_i ($i = 1, 2, \ldots, N_{\text{pixel}}$) form a set of pixels containing the entire path, we can write that

$$\Delta R' = \Delta R'\left(\bigcup_{i=1}^{N_{\text{pixel}}} B_i\right) = \sum_{i=1}^{N_{\text{pixel}}} F[\rho(B_i)] = \kappa \sum_{i=1}^{N_{\text{pixel}}} \log \rho(B_i). \tag{16}$$

Rearranging this equation gives

$$\kappa = \frac{\Delta R'}{\sum_{i=1}^{N_{\text{pixel}}} \log \rho(B_i)}, \tag{17}$$

and so substituting κ into equation (15) and then considering equation (12) yields

$$\Delta R'(B_j) = \frac{\Delta R'}{\sum_{i=1}^{N_{\text{pixel}}} \log \rho(B_i)} \log \rho(B_j), \tag{18a}$$

for any $j = 1, 2, \ldots, N_{\text{pixel}}$. Naturally, we cannot use this equation if the denominator is zero, which occurs when the overall 3-D effect along a path is zero. In this case the equality $\sum_{i=1}^{N_{\text{pixel}}} \log \rho(B_i) = 0$ implies that $\rho = \prod_{i=1}^{N_{\text{pixel}}} \rho(B_i) = 1$, and so we need to use the equation

$$\Delta R'(B_j) = \lim_{\rho \to 1} \Delta R'(B_j) = \log \rho(B_j) R'_{1\text{-D}}. \tag{18b}$$

This equation was obtained by using equations (6) and (10) in the following derivation:

$$\begin{aligned} \lim_{\rho \to 1} \Delta R'(B_j) &= \lim_{\rho \to 1} \frac{\Delta R'}{\sum_{i=1}^{N_{\text{pixel}}} \log \rho(B_i)} \log \rho(B_j) \\ &= \log \rho(B_j) \lim_{\rho \to 1} \frac{\Delta R'}{\log \prod_{i=1}^{N_{\text{pixel}}} \rho(B_i)} \\ &= \log \rho(B_j) \lim_{\rho \to 1} \frac{R'_{3\text{-D}} - R'_{1\text{-D}}}{\log \rho} \\ &= \log \rho(B_j) \lim_{\rho \to 1} \frac{\rho R'_{1\text{-D}} - R'_{1\text{-D}}}{\log \rho} \\ &= \log \rho(B_j) R'_{1\text{-D}} \lim_{\rho \to 1} \frac{\rho - 1}{\log \rho} = \log \rho(B_j) R'_{1\text{-D}}. \end{aligned} \tag{19}$$

[37] Let us note that we used e-based logarithm only for the sake of simplicity, as the normalization ensures that we get identical results for any logarithm base; that is, the method yields the single correct value for $\Delta R'(B_j)$. (If a different logarithm base (a) was used, equation (18b) would include the factor $\log_a e$, which is the limit in the last part of equation (19).)

[38] The statements below illustrate the proposed technique's properties that follow from equations (18a) and (18b). After each statement, a brief justification is also included in parentheses.

[39] 1. If B_j has the same properties as A, no 3-D effect will be attributed to B_j. (Because $\beta_{3\text{-D}}(B_j) = \beta_{1\text{-D}}(B_j)$ and $P_{3\text{-D}}(B_j) = P_{1\text{-D}}(B_j)$, equation (11) gives $\rho(B_j) = 1$. Then it follows from equations (18a) and (18b) that $\Delta R'(B_j) = 0$.)

[40] 2. If B_j reduces the radiation reaching A by a certain factor, and B_k (another pixel along the path; $k \neq j$) reduces it further by the same factor, the overall reduction will be distributed evenly between the two pixels. (It is clear from equations (18a) and (18b) that if $\rho(B_j) = \rho(B_k)$, then $\Delta R'(B_j) = \Delta R'(B_k)$.)

[41] 3. If B_j reduces the flow of radiation toward A by a factor of 2, and then B_k reduces it further by another factor of 2, their combined effect will be the same as the effect of a third pixel B_l along the path that reduces the flow by a factor of 4. (The values $\rho(B_j) = \rho(B_k) = 0.5$ and $\rho(B_l) = 0.25$ imply that $\log \rho(B_j \cup B_k) = \log \rho(B_j) + \log \rho(B_k) = \log \rho(B_l)$ (≈ -1.4), and so equations (18a) and (18b) yields $\Delta R'(B_j) + \Delta R'(B_k) = \Delta R'(B_l)$.)

[42] 4. If B_j reduces the radiation reaching A by a certain factor, and B_k enhances it by the same factor, their combined effect will be zero. (The equation $\rho(B_j) = 1/\rho(B_k)$ implies that $\log \rho(B_j) + \log \rho(B_k) = 0$, and so equations (18a) and (18b) yields $\Delta R'(B_j) + \Delta R'(B_k) = 0$.)

[43] 5. A pixel can have an enhancing effect even if the total 3-D effect along the path reduces the flow of radiation. In this case the enhancement acts by mitigating the reduction caused by other pixels along the path. (It is clear in equations (18a) and (18b) that if $\Delta R'$ and $\sum_{i=1}^{N_{\text{pixel}}} \log \rho(B_i)$ are both negative, $\Delta R'(B_j)$ remains positive if $\log \rho(B_j)$ is positive.)

[44] Once the magnitude of a pixel's influence is obtained from equations (18a) and (18b), the method can also identify the mechanism of 3-D effects caused by each pixel along each path. As mentioned in section 2.1, the mechanisms can be identified by considering whether the 3-D effects enhance or reduce the flow of radiation ($\rho > 1$ or $\rho < 1$) and whether they act by causing more scattering or less ($\beta_{3\text{-D}} > \beta_{1\text{-D}}$ or $\beta_{3\text{-D}} < \beta_{1\text{-D}}$). Therefore the influence of a pixel along a particular path can be attributed to one of the four basic mechanisms (defined in section 2.1 and illustrated in Figure 2):

[45] 1. EMS, if $\rho > 1$ and $\beta_{3\text{-D}} > \beta_{1\text{-D}}$,

[46] 2. ELS, if $\rho > 1$ and $\beta_{3\text{-D}} < \beta_{1\text{-D}}$,

[47] 3. RMS, if $\rho < 1$ and $\beta_{3\text{-D}} > \beta_{1\text{-D}}$, and

[48] 4. RLS, if $\rho < 1$ and $\beta_{3\text{-D}} < \beta_{1\text{-D}}$.

[49] Once the calculations have been done for all simulated paths, one can obtain a pixel's overall effect by combining the results calculated for each individual path using the equation

$$\Delta R^A(B) = \sum_{i=1}^{N_{\text{path}}} \Delta R'_i(B), \tag{20}$$

where N_{path} is the total number of simulated photon paths that were put into either the enhancement or reduction category.

[50] In the end, the contribution values calculated from equation (20) can be interpreted through the following two statements:

[51] 1. Summing up the influence of all pixels gives the overall 3-D effect, ΔR^A.

[52] 2. If pixel B has a contribution N times larger than pixel C does, then a set of N pixels having the same influence as C will have a combined effect equivalent to that of B.

3. Some Sample Results From the Proposed Technique

[53] This section describes some sample results that illustrate various ways in which the proposed method can be used to gain new knowledge about 3-D radiative effects. The photon paths used to obtain the numerical results of this paper were generated using the backward Monte Carlo model labeled "UMBC5" in the Intercomparison of 3-D Radiative Codes (I3RC) project (see http://climate.gsfc.nasa.gov/I3RC). This model was chosen because backward simulations are computationally more efficient for explaining the brightness of a particular pixel: Unlike forward simulations, they do not waste time simulating paths that do not lead to the pixel of our interest.

3.1. Case Studies

[54] This section describes some sample results for the cloud field used in case 3 of the I3RC project. The optical thickness field (Figure 4a) and cloud top height field were retrieved from Landsat measurements by the I3RC coordinators using 1-D radiative transfer and assuming a vertical temperature gradient of 5°C km^{-1}. The scene covers a (3.84 km)^2 area at 30-m resolution and assumes a constant cloud base and vertically constant volume extinction coefficient in each pixel. Clouds cover 88% of the scene, and the mean cloud optical thickness is 11. The calculations presented here assume no atmospheric effects, a nonreflecting surface, a Henyey-Greenstein scattering phase function, and a 60° solar zenith angle with the Sun on the left. The exact parameters of the scene (including all pixel values) are available at http://climate.gsfc.nasa.gov/I3RC.

[55] Figure 4b shows how various pixels influence the brightness of an arbitrarily selected pixel A at row 57, column 90. Let us note that the values in the map are very small because each number represents the contribution of an individual (30 m)^2 pixel. Summed up over the entire scene, these values give the overall 3-D effect of $\Delta R^A = 0.128$ ($R^A_{1\text{-D}} = 0.574$, $R^A_{3\text{-D}} = 0.702$). The figure reveals that most of the 3-D effects are caused by the thin pixels right in front of A and by the cloud bump right behind it. This is because (just as in 1-D clouds) the scattering phase function's forward and backward peaks allow most photons to travel near the solar azimuth even after several scattering events. Still, even pixels farther away have a discernible impact: In front, thin pixels (B, C) enhance R^A by means of ELS, whereas to the sides and behind, thick pixels (D) increase R^A through EMS and thin pixels (E, F) reduce it through RLS.

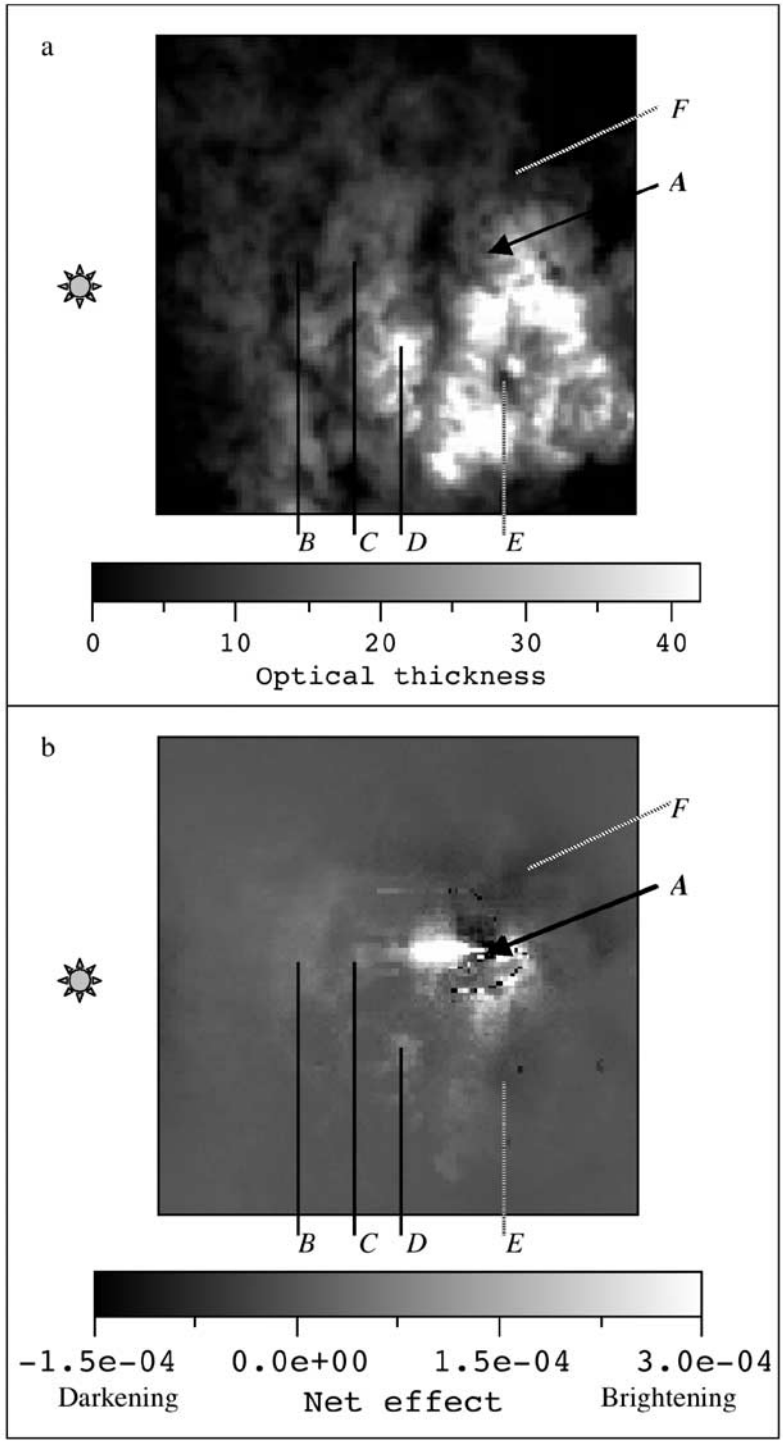

Figure 4. (a) Optical thickness distribution of the I3RC case 3 cloud field. (b) Contribution of various pixels to the overall 3-D effect influencing the brightness of pixel *A*. See text for a discussion of how pixels *B*-*F* influence the brightness of pixel *A*. See color version of this figure at back of this issue.

[56] In addition to examining 3-D effects that influence individual pixels, the proposed method can also be used to get scene-averaged results by simply combining results that were obtained by moving the position of the influenced pixel across the scene. Table 1 displays the results of such a calculation regarding the magnitude of various 3-D mechanisms. The results reveal that, perhaps somewhat surprisingly, the strongest mechanism in this scene is RLS, whereas the weakest one is RMS. Also, smoothing is somewhat stronger than roughening, which means that influencing pixels have a slight tendency to modify their surroundings' reflectance by nudging them closer to their own 1-D reflectance. These findings agree with the tendencies in earlier studies that reported strong

Table 1. Scene-Averaged Magnitude of Various 3-D Mechanisms

Mechanism	Magnitude
EMS	0.182
RMS	−0.132
ELS	0.329
RLS	−0.345
Smoothing	0.527
Roughening	0.461
Overall 3-D effect	0.034

smoothing and leakage effects [e.g., *Chambers et al.*, 1997b].

[57] We can learn further details on smoothing and roughening if we plot how much net roughening (= roughening − smoothing) is caused by pixels at various distances from the influenced pixels. Figure 5 shows that for the scene in Figure 4a roughening works primarily in the solar plane (that is, pixels tend to experience roughening effects from pixels in front of them), whereas smoothing is much more isotropic. The difference confirms that roughening acts mainly by influencing the pixels' illumination by direct and low-order scattered sunlight, whereas smoothing is caused by diffusion due to multiple scattering. This interpretation agrees well with the assertion of earlier studies [e.g., *Zuidema and Evans*, 1998] that roughening is strongest for oblique Sun (when the surroundings can change a pixel's illumination), whereas diffusive smoothing works at all solar elevations. Also, the result is consistent with the results in *Várnai* [2000], which show that 3-D effects make the reflectance field anisotropic, with stronger variability in the along-Sun than in the cross-Sun direction.

3.2. Statistical Results

[58] In addition to allowing detailed case studies of individual scenes, the proposed method can also provide statistical information for large sets of scenes. Fortunately, these calculations do not take longer than the calculations for individual scenes: In most cases we can build accurate statistics by combining quick, noisy results obtained for individual scenes. Such statistical results can be important in practical applications, particularly in the development of new radiative transfer parameterizations for either remote sensing or dynamical cloud models.

[59] To illustrate the kind of results the method can give, some sample calculations were performed to examine how pixels with $\tau = 10$ are influenced by pixels with $\tau = 5$ and $\tau = 15$ around them. For this, 5000 cloud fields were generated using the third fractal cloud model described in the work of *Várnai and Marshak* [2001], which is based on the model of *Evans* [1993]. This model starts by generating cloud structures using Fractional Brownian Motion [e.g., *Mandelbrot*, 1982; *Barker and Davies*, 1992], and then it exponentiates the pixel values so that the cloud fields have plausible, skewed histograms and more realistic fractal properties. The goal was not to provide climatologically representative statistics but only to cover a wide but realistic range of cloud properties. Although all scenes cover $(12.8\ \text{km})^2$ areas at 100 m resolution, they have a constant cloud base and a constant volume scattering coefficient of $30\ \text{km}^{-1}$ and use the I3RC C.1 scattering phase function; the other scene parameters were chosen randomly for each scene between the limits listed in Table 2. Next, 4% of all pixels with $9.75 < \tau < 10.25$ were selected from each of the scenes, and one thousand 1-D and one thousand 3-D photon paths were simulated for each selected pixel. The results were then combined for all pixels and stored as a function of various parameters.

[60] As a sample result, Figure 6 shows the role of the pixels' position relative to each other. Figure 6a quantifies the intuitive trend that thin pixels in front enhance a pixel's brightness whereas thin pixels behind reduce it, and Figure 6b shows that the trends reverse for thick pixels. In addition, the figure shows that the pixels' influence on each other drops much more quickly with their distance in the cross-Sun direction than with their distance in the along-Sun direction. This is because radiation arriving from the Sun travels mainly in the along-Sun direction before multiple scattering can direct some of it into cross-Sun directions. Also, the comparison of Figures 6a and 6b reveals that τ changes of the same magnitude ($|\Delta\tau| = 5$) have stronger radiative effects if the pixel in front is thicker rather than thinner. Finally, the figure reveals that (especially in slopes facing away from the Sun) the same τ difference is more effective if it occurs over larger distances, that is, in less steep slopes. On sunlit slopes, this is because too steep slopes allow some incoming direct radiation to descend to such low altitudes that it needs to travel some more

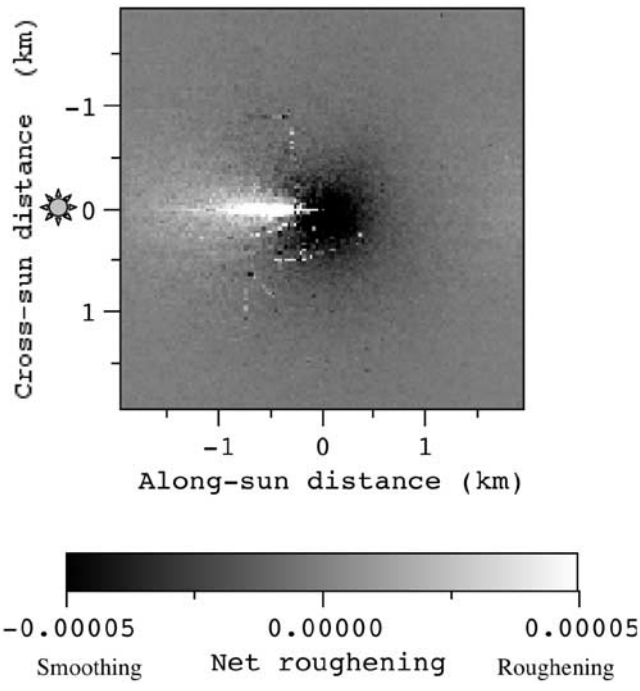

Figure 5. Scene-averaged map of net roughening (= roughening − smoothing) in the cloud field shown in Figure 4a. The net roughening values are shown as a function of the influencing pixels' position relative to the influenced pixel; negative and positive along-Sun distances indicate that the net roughening is caused by pixels in front of or behind the influenced pixel, respectively. See color version of this figure in the HTML.

Table 2. Limits for Various Statistical Cloud Parameters

Parameter	Limit
Hölder exponent (H) [*Mandelbrot*, 1982]	0.3–0.45
Probability of overcast scenes	0.2
Cloud fraction for broken cloud scenes	0.3–1.0
Scene-averaged optical thickness	5–15
ν(=mean/standard deviation)	4–25 for overcast scenes, 1–5 for broken cloud scenes

horizontal distance before it can turn around and emerge from the cloud top. On slopes facing away from the Sun, too steep cloud bumps are less effective because they not only shadow our pixel but also steer some such radiation toward it that would have passed over the top of our pixel without the bump's interference.

3.3. Parameterizations

[61] The most important benefit of the new method's statistical results will perhaps be the development of new radiative parameterizations. The new parameterizations could incorporate 3-D radiative effects into practical applications that are currently limited to 1-D radiative transfer theory, such as dynamical cloud modeling and remote sensing. In one possible approach, new parameterizations would estimate the needed radiative quantity at each pixel in three steps:

[62] 1. Calculate an initial estimate using 1-D theory.

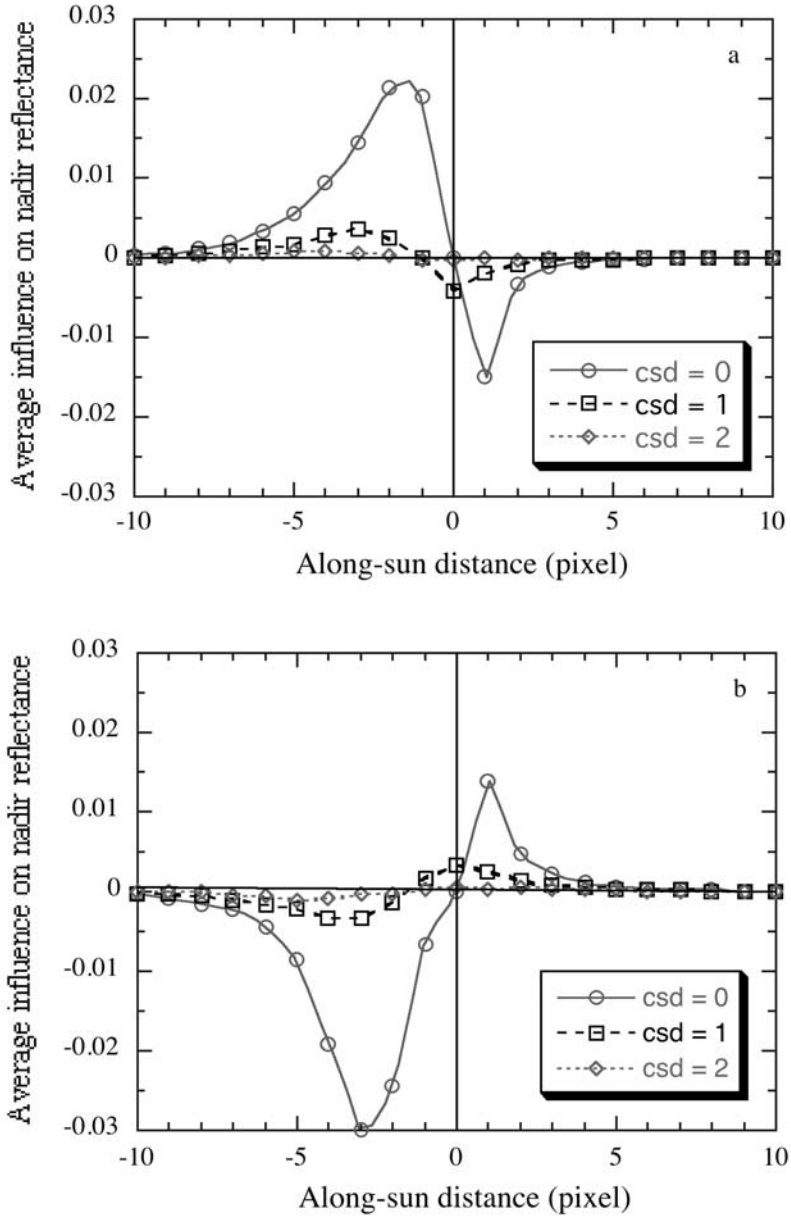

Figure 6. Average influence of pixels with (a) $\tau = 5$ and (b) $\tau = 15$ on pixels with $\tau = 10$. Negative distances indicate that the influencing pixel is in front of the influenced one. The three lines show results for three different cross-Sun distance (csd) values (in pixels) between the influenced and influencing pixels. See color version of this figure in the HTML.

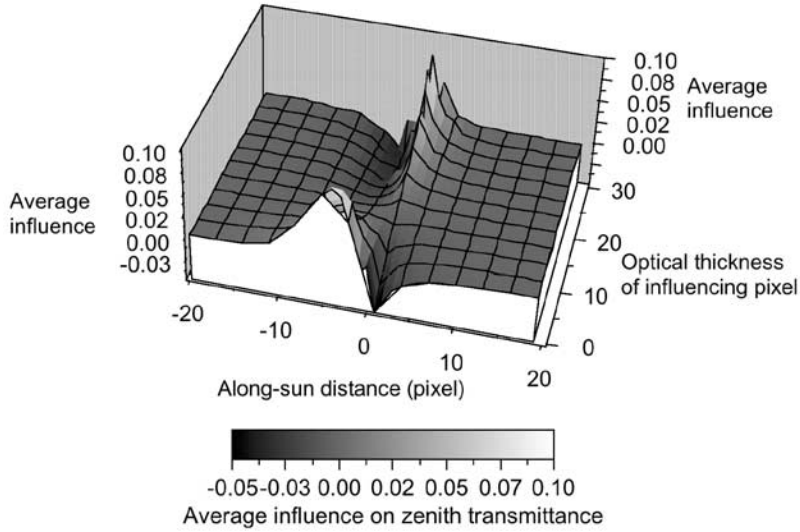

Figure 7. Average influences on the zenith transmittance of pixels with $\tau = 10$. The influence values are displayed as a function of the relative position and the optical thickness of the influencing pixel. Negative distances indicate that the influencing pixel is in front of the influenced one. The results were obtained for 60° solar zenith angle, assuming 2-D radiative transfer in a large set of vertically constant, flat-topped clouds. See color version of this figure at back of this issue.

[63] 2. Use the new statistical relationships (e.g., Figure 7) to estimate what 3-D effect each nearby pixel causes.

[64] 3. Sum up the estimated influences of all nearby pixels and combine them with the original 1-D estimate, thus yielding our final result. For example,

$$R_{3\text{-D}}^{\text{estim}}(A) = R_{1\text{-D}}(A) + c \sum_i \Delta R^A(B_i), \qquad (21)$$

where the summation goes over all potentially relevant (nearby) pixels, and c is an empirical regression coefficient that may depend on known factors such as radiative quantity or spatial resolution but certainly not on the cloud characteristics in individual scenes.

[65] We tested the viability of this approach on several Landsat images containing a variety of cloud types. As input to the tests, we used the optical thickness fields retrieved using 1-D theory for scenes 12, 38, 39, 40, 43, and 49 of *Harshvardhan et al.* [1994] (courtesy of Bruce Wielicki and Lindsay Parker). Assuming a solar zenith angle of 60°, the tests compared the estimations of nadir reflectance and zenith transmittance to accurate values obtained from 3-D Monte Carlo simulations. Figure 7 illustrates the statistical results used for the parameterizations of zenith transmittance. The figure reveals that thin and thick areas in front tend to enhance and reduce a pixel's transmittance, respectively, and that this tendency is reversed for areas behind. Figure 8 shows the parameterization results for zenith transmittance, a quantity that proved more difficult to estimate than nadir reflectance in a neural network approach [*Fauré et al.*, 2001c].

[66] While recognizing that our initial test cases were relatively simple (they assumed 2-D radiative transfer in vertically constant, flat-topped clouds), we were very much encouraged by the results, for two reasons. First, the results suggest that the method will be able to provide fast and fairly accurate estimations for a variety of cloud types. (Let us note that the artificial scenes used to establish the statistical relationships in Figure 7 simply covered a wide range of realistic cloud parameters; they were not tailored to the clouds in Figure 8.) Second, the current estimations used simple statistical relationships that considered only the optical thicknesses of the influenced and influencing pixels and their position relative to each other. This implies that, if needed, the accuracy can be improved by considering additional information about other nearby pixels. For example, considering the optical thickness of other pixels in between could help because one pixel's influence on another tends to be weaker if the pixels in between are less transparent.

[67] Let us mention that the parameterizations consider influences up to a certain maximum distance, which may depend on factors such as cloud thickness and solar zenith angle. Fortunately, choosing too large maximum distances can never cause parameterization errors, it only makes the calculations slower. Thus the choice of maximum distance offers researchers one simple way to set the balance between speed and accuracy according to their needs.

[68] The parameterization approach described above can be adopted easily for applications in which the true cloud structure is known, such as dynamical cloud modeling. (The only modification required for incorporating absorption is to replace the scattering coefficient by the extinction coefficient in the first (exponential) term of equations (7) and (9)–(11).) Although in remote sensing applications the true cloud properties are not known a priori, the parameterizations may still be useful in either one of the following two approaches.

[69] The first, iterative approach has already been tried by researchers who used existing 3-D radiative transfer calculation methods, such as Monte Carlo. However, the slowness of 3-D calculations has prevented the thorough testing and wide use of this approach, a problem that may be alleviated by the new parameterizations. In this approach we

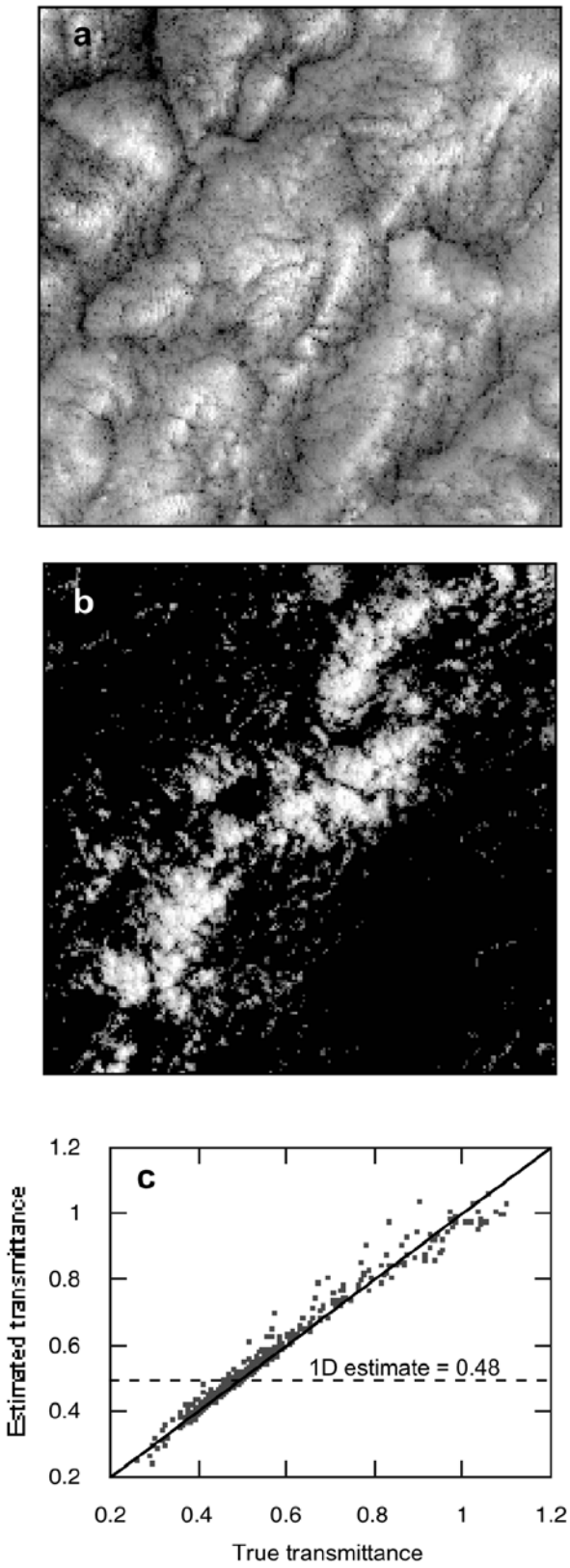

start with a 1-D retrieval of cloud properties (e.g., τ_{retr}) from the observed reflectances (R_{obs}). Then we use the parameterizations above to calculate (including 3-D effects) the radiances R_{param} that would emerge from the 1-D-retrieved field τ_{retr}. By comparing R_{param} and R_{obs}, we can improve upon the original, 1-D estimates. For example, if $R_{param} < R_{obs}$, we increase τ_{retr}. Then the improvements of τ_{retr} can be repeated in subsequent iteration steps until the fields of R_{param} and R_{obs} become sufficiently similar. The second approach to using the parameterizations in remote sensing would tabulate the statistical results not as a function of true cloud properties (e.g., τ in Figure 7) but as a function of observable radiance values. For example, similar to the retrievals of *Fauré et al.* [2001b] and *Várnai and Marshak* [2002], the parameterizations could use the visible and infrared radiances observed at a pixel and in its surroundings for estimating 3-D effects at the pixel (ΔR). Then we could remove the influence of 3-D effects from our observations using $R_{1\text{-}D} = R_{obs} - \Delta R$ and perform accurate 1-D retrievals based on the "corrected" $R_{1\text{-}D}$ fields.

4. Summary

[70] This paper proposed a method for obtaining new information on 3-D radiative effects arising from horizontal radiative interactions in heterogeneous clouds. The goal was to overcome a limitation of current radiative transfer models that can calculate only how 3-D effects change radiative quantities at any given pixel (for example, the pixel's visible brightness) but cannot quantitatively address questions about their causes, such as the following: Why is a certain pixel as bright as it is? What other pixels influence its brightness, to what degree, and through what mechanisms?

[71] The proposed method can address such questions by detecting 3-D effects directly as they modify the flow of radiation inside the cloud field. As a result, it can not only calculate the combined effect a pixel's surroundings have on its brightness but can also determine how specific pixels contribute to the combined effect, to what degree, and through what mechanisms.

[72] The proposed method recognizes the fact that the pixels causing 3-D effects do not act in isolation, because a pixel's influence also depends on other pixels along the path of radiation. For example, a pixel can strongly affect another one if the pixels between them are transparent, but it cannot make much of a difference if the pixels in between are so dense that they hardly allow any radiation through. This implies that the influence of pixel *B* on pixel *A* should be determined considering not only the properties

Figure 8. (opposite) (a and b) Two of the six examined Landsat images that cover (30 km)^2 areas at 60-m resolution (courtesy of Bruce Wielicki). (c) Comparisons of the accurate and the estimated zenith transmittance values for 1348 randomly selected pixels that have optical thicknesses close to 10. The results are from 2-D calculations, and they assumed a constant geometrical cloud thickness of 400 m (no vertical variability) and a solar zenith angle of 60°. The dashed line indicates that 1-D methods would estimate a zenith transmittance value of approximately 0.48 for all these pixels. See color version of this figure in the HTML.

of B and A but also the entire paths along which the radiation arrives from the Sun, moves to B, and then goes to A. Unfortunately, explicit solutions to the equation of radiative transfer, such as the Spherical Harmonics Discrete Ordinate Method (SHDOM) of *Evans* [1998], can give information only on radiative quantities at fixed locations (e.g., the spatial and angular distribution of radiance values), but they cannot provide the paths radiation follows. Therefore the proposed method uses Monte Carlo experiments that can simulate the photons' journey inside any cloud field (even in multilayer cloud systems).

[73] The paper defined the contribution of each pixel to the overall 3-D effect such that the contribution values can be interpreted through the following two statements. First, summing up the contribution of all pixels gives the overall 3-D effect. Second, if pixel B has a contribution N times larger than pixel C, then N pixels having the same influence as C will have a combined effect equivalent to that of B.

[74] In addition, the method identifies the mechanism of 3-D effects caused by each pixel. For this, the paper provided quantitative definitions for 3-D processes that were described qualitatively in earlier studies, for effects both on individual pixels (e.g., side illumination or shadowing) and on the structure of entire scenes (i.e., smoothing and roughening).

[75] After describing the proposed method, the paper illustrated its new capabilities through several examples. First, a cloud field used in the I3RC project was examined in detail: 3-D effects influencing a particular pixel were mapped out, and their mechanisms were calculated. These sample results provided some new insights, for example, that shadowing (termed here as "reduction by more scattering") was the weakest 3-D mechanism even for a solar zenith angle of 60°.

[76] After the detailed case study, some statistical results were presented for large sets of scenes. The results illustrated how the influence of one pixel on another depends on the pixels' positions relative to each other. Among other findings, the results revealed that the strongest 3-D effects act near the solar azimuth. This implies that in order to take 3-D effects into account, the interpretation of remote sensing measurements will need to focus mainly on the pixels in front and behind a given pixel [see *Várnai and Marshak*, 2002], whereas sideways, they will need to consider only the fairly close neighbors. Let us note that the distances required for the (≈300 m thick) clouds examined here will vary in future studies because 3-D effects can act over larger distances in thicker clouds [e.g., *Davis et al.*, 1997] and because cloud phase, solar zenith angle, and other factors also influence how far photons can travel inside a cloud.

[77] Perhaps it is in generating such statistical results that the proposed method may be most useful in future studies: Because the method can link a cause to its effect for the first time (i.e., link a particular change in cloud properties to the resulting 3-D radiative effect), it can be used in developing new radiative transfer parameterizations. Initial work has already begun to develop such parameterizations, and the paper presented some preliminary results for a variety of cloud types. On the basis of the encouraging results, we hope that in future studies, such parameterizations will be able to incorporate 3-D effects into practical applications that are currently limited to 1-D theory, for example, into the remote sensing of cloud properties or into dynamical cloud modeling.

[78] **Acknowledgments.** We are grateful to Laura Atwood and Raymond M. Hoff for reading the manuscript and providing helpful suggestions. We appreciate funding for this research from the NASA EOS Project Science Office (under grant NAG5-6675) and support from project scientist David O'C. Starr.

References

Barker, H. W., and J. A. Davies, Solar radiative fluxes for stochastic, scale-invariant broken cloud fields, *J. Atmos. Sci.*, *49*, 1115–1126, 1992.

Barker, H. W., J.-J. Morcrette, and G. D. Alexander, Broadband solar fluxes and heating rates for atmospheres with 3-D broken clouds, *Q. J. R. Meteorol. Soc.*, *124*, 1245–1271, 1998.

Benner, T., and K. F. Evans, Three-dimensional solar radiative transfer in small tropical cumulus fields derived from high-resolution imagery, *J. Geophys. Res.*, *106*, 14,975–14,984, 2001.

Busygin, V. P., N. A. Yevstratov, and Ye. M. Feygelson, Optical properties of cumulus clouds, and radiative fluxes for cumulus cloud cover, *Izv. Russ. Acad. Sci. Atmos. Oceanic Phys., Engl. Transl.*, *9*, 648–653, 1973.

Cahalan, R. F., W. L. Ridgway, and W. J. Wiscombe, Independent pixel and Monte Carlo estimates of stratocumulus albedo, *J. Atmos. Sci.*, *51*, 3776–3790, 1994.

Cannon, J. C., Line transfer in two dimensions, *Astrophys. J.*, *161*, 255–264, 1970.

Chambers, L. H., B. A. Wielicki, and K. F. Evans, Independent pixel and two-dimensional estimates of Landsat-derived cloud field albedo, *J. Atmos. Sci.*, *54*, 1525–1532, 1997a.

Chambers, L. H., B. A. Wielicki, and K. F. Evans, Accuracy of the independent pixel approximation for satellite estimates of oceanic boundary layer cloud optical depth, *J. Geophys. Res.*, *102*, 1779–1794, 1997b.

Davies, R., The effect of finite geometry on the three-dimensional transfer of solar irradiance in clouds, *J. Atmos. Sci.*, *35*, 1712–1725, 1978.

Davies, R., W. L. Ridgway, and K.-E. Kim, Spectral absorption of solar radiation in cloudy atmospheres: A 20 cm-1 model, *J. Atmos. Sci.*, *41*, 2126–2137, 1984.

Davis, A. B., and A. Marshak, Multiple scattering in clouds: Insights from three-dimensional diffusion/P_1 theory, *Nucl. Sci. Eng.*, *137*, 251–280, 2001.

Davis, A. B., A. Marshak, R. F. Cahalan, and W. J. Wiscombe, The Landsat scale break in stratocumulus as a three-dimensional radiative transfer effect: Implications for cloud remote sensing, *J. Atmos. Sci.*, *54*, 241–260, 1997.

Di Girolamo, L., T. Várnai, and R. Davies, Apparent breakdown of reciprocity in reflected solar radiances, *J. Geophys. Res.*, *103*, 8795–8803, 1998.

Evans, K. F., Two-dimensional radiative transfer in cloudy atmospheres: The spherical harmonic spatial grid method, *J. Atmos. Sci.*, *50*, 3111–3124, 1993.

Evans, K. F., The spherical harmonics discrete ordinate method for three-dimensional atmospheric radiative transfer, *J. Atmos. Sci.*, *55*, 429–446, 1998.

Fauré, T., H. Isaka, and B. Guillemet, Neural network analysis of the radiative interaction between neighboring pixels in inhomogeneous clouds, *J. Geophys. Res.*, *106*, 14,465–14,484, 2001a.

Fauré, T., H. Isaka, and B. Guillemet, Neural network retrieval of cloud parameters of inhomogeneous and fractional clouds: Feasibility study, *Remote Sens. Environ.*, *77*, 123–138, 2001b.

Fauré, T., H. Isaka, and B. Guillemet, Mapping neural network computation of high-resolution radiant fluxes of inhomogeneous clouds, *J. Geophys. Res.*, *106*, 14,961–14,973, 2001c.

Harshvardhan, B. A. Wielicki, and K. M. Ginger, The interpretation of remotely sensed cloud properties from a model parameterization perspective, *J. Clim.*, *7*, 1987–1998, 1994.

Kobayashi, T., Effects due to cloud geometry on biases in the cloud albedo derived from radiance measurements, *J. Clim.*, *6*, 120–128, 1993.

Loeb, N. G., and R. Davies, Observational evidence of plane parallel model biases: Apparent dependence of cloud optical depth on solar zenith angle, *J. Geophys. Res.*, *101*, 1621–1634, 1996.

Los, A., M. van Weele, and P. G. Duynkerke, Actinic fluxes in broken cloud fields, *J. Geophys. Res.*, *102*, 4257–4266, 1997.

Mandelbrot, B., *The Fractal Geometry of Nature*, 460 pp., W. H. Freeman, New York, 1982.

Marchuk, G. I., G. A. Mikhailov, M. A. Nazaraliev, R. A. Darbinjan, B. A. Kargin, and B. S. Elepov, *The Monte Carlo Methods in Atmospheric Optics*, 208 pp., Springer-Verlag, New York, 1980.

Marshak, A., A. Davis, W. Wiscombe, and R. Cahalan, Radiative smoothing in fractal clouds, *J. Geophys. Res.*, *100*, 26,247–26,261, 1995.

Marshak, A., W. Wiscombe, A. Davis, L. Oreopoulos, and R. F. Cahalan, On the removal of the effect of horizontal fluxes in two-aircraft measurements of cloud absorption, *Q. J. R. Meteorol. Soc.*, *125*, 2153–2170, 1999.

McKee, T. B., and S. K. Cox, Scattering of visible radiation by finite clouds, *J. Atmos. Sci.*, *31*, 1885–1892, 1974.

O'Hirok, W., and C. Gauthier, A three-dimensional radiative transfer model to investigate the solar radiation within a cloudy atmosphere, part I, Spatial effects, *J. Atmos. Sci.*, *55*, 2162–2179, 1998.

Oreopoulos, L., A. Marshak, R. F. Cahalan, and G. Wen, Cloud three-dimensional effects evidenced in Landsat spatial power spectra and autocorrelation functions, *J. Geophys. Res.*, *105*, 14,777–14,788, 2000.

Várnai, T., Influence of three-dimensional radiative effects on the spatial distribution of shortwave cloud reflection, *J. Atmos. Sci.*, *57*, 216–229, 2000.

Várnai, T., and R. Davies, Effects of cloud heterogeneities on shortwave radiation: Comparison of cloud-top variability and internal heterogeneity, *J. Atmos. Sci.*, *56*, 4206–4223, 1999.

Várnai, T., and A. Marshak, Statistical analysis of the uncertainties in cloud optical depth retrievals caused by three-dimensional radiative effects, *J. Atmos. Sci.*, *58*, 1540–1548, 2001.

Várnai, T., and A. Marshak, Observations of three-dimensional radiative effects that influence MODIS cloud optical thickness retrievals, *J. Atmos. Sci.*, *59*, 1607–1618, 2002.

Wendling, P., Albedo and reflected radiance of horizontally inhomogeneous clouds, *J. Atmos. Sci.*, *34*, 642–650, 1977.

Zuidema, P., and K. F. Evans, On the validity of the independent pixel approximation for the boundary layer clouds observed during ASTEX, *J. Geophys. Res.*, *103*, 6059–6074, 1998.

A. Marshak, Climate and Radiation Branch, NASA Goddard Space Flight Center, Greenbelt, MD 20771, USA.

T. Várnai, Joint Center for Earth Systems Technology, University of Maryland, Baltimore, MD 20771, USA. (varnai@climate.gsfc.nasa.gov)

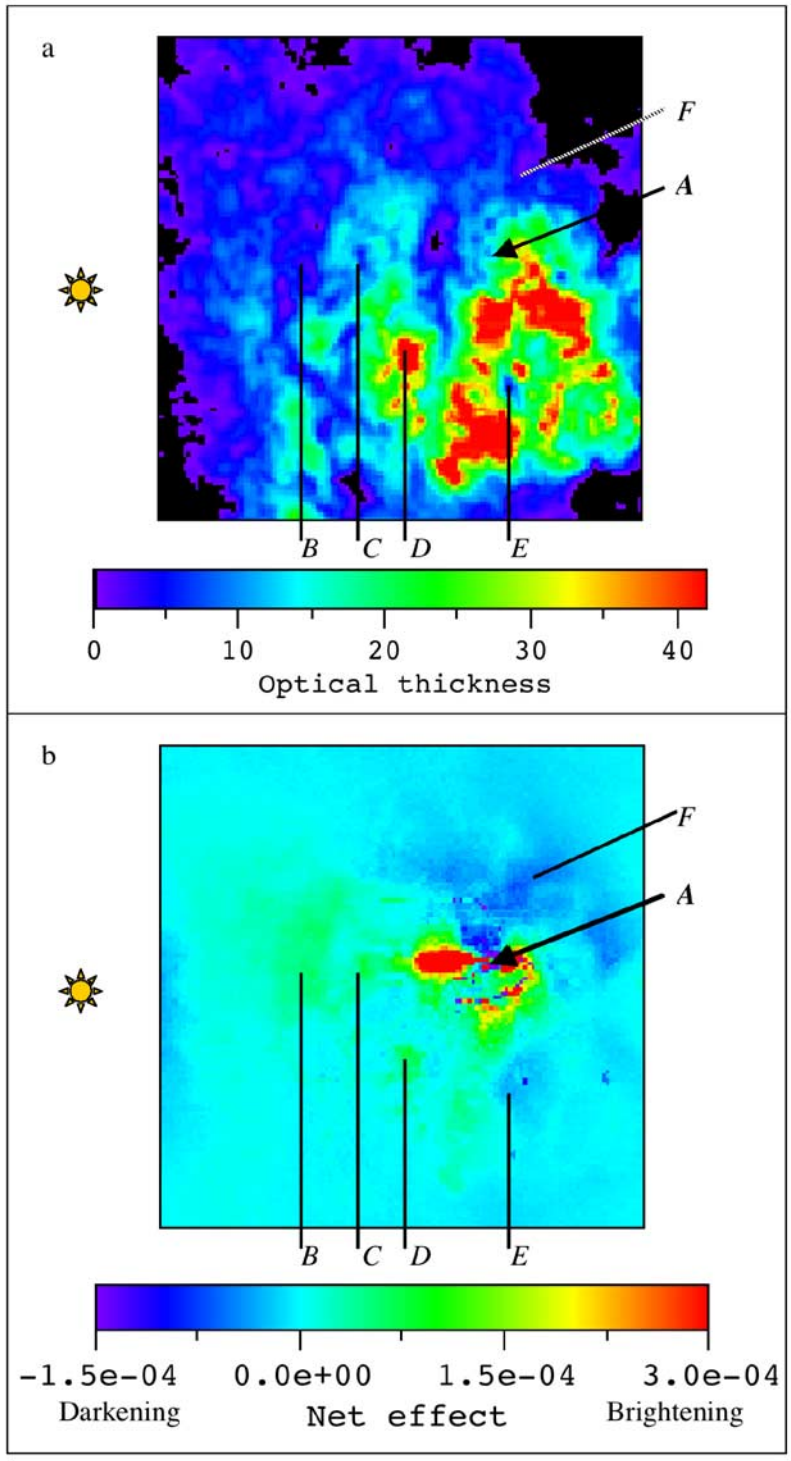

Figure 4. (a) Optical thickness distribution of the I3RC case 3 cloud field. (b) Contribution of various pixels to the overall 3-D effect influencing the brightness of pixel *A*. See text for a discussion of how pixels *B-F* influence the brightness of pixel *A*.

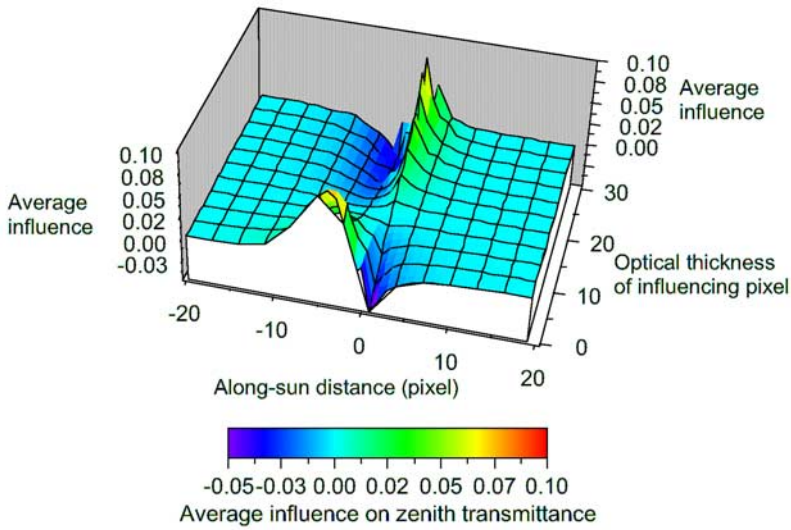

Figure 7. Average influences on the zenith transmittance of pixels with $\tau = 10$. The influence values are displayed as a function of the relative position and the optical thickness of the influencing pixel. Negative distances indicate that the influencing pixel is in front of the influenced one. The results were obtained for 60° solar zenith angle, assuming 2-D radiative transfer in a large set of vertically constant, flat-topped clouds.